Tellus (1990), *42A*, 594–604

On the structure of inertial western boundary currents with two moving layers

By RUI XIN HUANG, *Department of Physical Oceanography, Woods Hole Oceanographic Institution, Woods Hole, Massachusetts 02543, USA*

(Manuscript received 14 March 1989; in final form 4 September 1989)

ABSTRACT

The structure of inertial western boundary currents with two moving layers is studied using a streamfunction coordinate transformation. This transformation converts the equation system, a stiff system over a semi-infinite domain in physical coordinates, into a non-stiff system over a finite domain in streamfunction coordinates. For simplicity, the interfacial slopes of the interior solution are assumed constant. The structure of the solutions can be classified into three categories in a phase plane which consists of two regions joining along a critical line. Within each region, solutions of the system appear in the form of two unconnected branches. As parameters approach values corresponding to those at the critical line, the two branches of the solutions join at a movable critical point to form a continuous solution. Although changes in the vorticity profile of the incoming flow or other parameters can alter the position and shape of the critical line, the general features of the system remain unchanged. Thus, requiring continuity of an inertial western boundary current through a critical point, implies certain constraints on the structure of the mid-ocean thermocline.

1. Introduction

During the past 10 years, the theory of the ideal-fluid thermocline has evolved rapidly. Now we can calculate the three-dimensional structure of the subtropical interior using either a multi-layered model (Luyten et al., 1983) or a continuously stratified model (Huang, 1988). One of the deficiencies of these models is their inability to satisfy some essential lateral boundary conditions for a closed basin. Therefore, matching a solution of the interior ideal-fluid thermocline with a boundary current near the western wall would be an important step forward. Observations suggest that western boundary currents (especially the southern part) are predominantly inertial. Therefore, the most appealing approach is to close the ideal-fluid thermocline solution with an inertial boundary current near the western wall.

Although a one-moving-layer inertial model of the Gulf Stream (Stommel, 1954; Charney, 1955) reproduced the basic structure observed in the ocean fairly well, so far multi-layer models have not been successful. Blandford (1965), in attempting to solve the structure of inertial western boundary currents with two moving layers, found analytical solutions for cases of constant potential vorticity in both moving layers. His results showed an inexplicable, abrupt separation of the upper layer at latitudes much lower than the separation latitude corresponding to the one-moving-layer model. Numerical results for the general cases of non-constant potential vorticity were also included in his thesis (Blandford, 1964); the results were similar to the constant potential vorticity cases and no smooth solutions were found. The failure of the two-moving-layer model of inertial western boundary currents has caused serious concern about whether a purely inertial western boundary current for a multi-layer or continuously stratified system is possible.

Luyten and Stommel (1985) explained the paradoxical situation in terms of the virtual control phenomenon first found in the one-dimensional hydraulic problem by Wood (1968). According to their theory, specifying the interior thermocline structure in terms of layer depth leads to an overdetermined problem, in which discontinuities in solutions are inevitable. To demonstrate the basic idea, Luyten and Stommel used a zero potential vorticity model in which all water comes from the equator. However, the Gulf Stream is fed from middle latitudes, not the equator, and the potential vorticity is non-zero. Thus, it is important to examine the structure of an inertial boundary layer of non-zero potential vorticity. Since Blandford had shown that no continuous solution is possible for the case of uniform potential vorticity, we will search for possible continuous solutions by gradually changing the potential vorticity gradient. Furthermore, if continuous solutions exist, we will try to find out how they change in response to the parameter change.

2. Formulation

We consider a β-plane ocean, in which two layers of constant density ρ_1 and ρ_2 move over a third stagnant layer of density ρ_3. Assuming the zonal velocity is much smaller than the meridional velocity, we have the basic equations of a two-and-a-half-layer model of the inertial western boundary current (cf. Blandford, 1965)

$$-fv_1 = -g'(\gamma h_{1x} + h_{2x}), \tag{2.1}$$

$$u_1 v_{1x} + v_1 v_{1y} + fu_1 = -g'(\gamma h_{1y} + h_{2y}), \tag{2.2}$$

$$(h_1 u_1)_x + (h_1 v_1)_y = 0, \tag{2.3}$$

$$-fv_2 = -g'(h_{1x} + h_{2x}), \tag{2.4}$$

$$u_2 v_{2x} + v_2 v_{2y} + fu_2 = -g'(h_{1y} + h_{2y}), \tag{2.5}$$

$$(h_2 u_2)_x + (h_2 v_2)_y = 0, \tag{2.6}$$

where $f = f_0 + \beta y$ is the Coriolis parameter, $(h_i, u_i, v_i; i = 1, 2)$ are the layer thickness and horizontal velocity, $g' = [(\rho_3 - \rho_2)/\bar{\rho}]g$ is the reduced gravity, $\bar{\rho}$ is the reference density, $\gamma = (\rho_3 - \rho_1)/(\rho_3 - \rho_2)$, and subscripts x, y indicate partial derivatives. This system conserves potential vorticity

$$\frac{v_{1x} + f}{h_1} = F_1(\psi_1), \tag{2.7}$$

$$\frac{v_{2x} + f}{h_2} = F_2(\psi_2), \tag{2.8}$$

and Bernoulli function

$$\frac{1}{2} v_1^2 + g'(\gamma h_1 + h_2) = G_1(\psi_1), \tag{2.9}$$

$$\frac{1}{2} v_2^2 + g'(h_1 + h_2) = G_2(\psi_2), \tag{2.10}$$

where ψ_1 and ψ_2 are streamfunctions in the upper and lower layer defined so that

$$\psi_{ix} = h_i v_i, \quad (i = 1, 2), \tag{2.11}$$

$$\psi_{iy} = -h_i u_i, \quad (i = 1, 2). \tag{2.12}$$

$F_1(\psi_1)$, $F_2(\psi_2)$, $G_1(\psi_1)$, and $G_2(\psi_2)$ are known functions of the streamfunctions ψ_1 and ψ_2, calculated from the specified incoming flow. In addition, there is a simple integral connecting the barotropic streamfunction with the layer thicknesses

$$\begin{aligned}(\psi_{1\infty} + \psi_{2\infty}) - (\psi_1 + \psi_2) &= \frac{g'}{f}\left[\frac{\gamma}{2}(h_{1\infty}^2 - h_1^2) + h_{1\infty}h_{2\infty} - h_1 h_2 \right.\\ &\quad \left. + \frac{1}{2}(h_{2\infty}^2 - h_2^2)\right],\end{aligned} \tag{2.13}$$

where $\psi_{1\infty}$, $\psi_{2\infty}$, $h_{1\infty}$, and $h_{2\infty}$ are the corresponding values of the mid-ocean thermocline.

Using (2.1) and (2.4), (2.7) and (2.8) can be rewritten as a pair of second-order ordinary differential equations for layer thicknesses h_1 and h_2,

$$\gamma h_{1xx} + h_{2xx} - \frac{f}{g'} F_1(\psi_1) h_1 = \frac{f^2}{g'}, \tag{2.14}$$

$$h_{1xx} + h_{2xx} - \frac{f}{g'} F_2(\psi_2) h_1 = \frac{f^2}{g'}. \tag{2.15}$$

Generally, F_1 and F_2 in (2.14, 2.15) are not constant, thus (2.11) has to be solved at the same time as (2.14, 2.15) are solved (Blandford, 1965). The problem requires solving six first-order ordinary differential equations simultaneously. Unfortunately, this equation system is very stiff. (For stiff equations and numerical methods solving them, see Gear, 1971.) Physically, the system possesses solutions which grow or decay exponentially. For multi-layered models, baroclinic modes generally have horizontal scales much smaller than the barotropic mode, so that some components of the inertial western boundary currents can decay quickly within a short distance of the order of the baroclinic Rossby deformation radius, while the entire solution extends from the western wall to infinity (the interior). Furthermore, some boundary conditions are posed at infinity. The numerical difficulties of handling such a problem are severe. Although Blandford tried to solve the problem with the best package available at that time, it was very hard to find solutions with satisfactory accuracy, especially at large distance from the coast. (The numerical difficulties involved in solving this stiff system might be the major reason why Blandford could not find any continuous solution.) I have tried, without much success, to solve the problem using several numerical methods, including the well-documented subroutine in the IMSL mathematical software library specially designed for solving stiff equations by the Gear method.

These difficulties may be overcome by a coordinate transformation. In the present case, the von Mises (1927) transformation is very useful. In fact, Charney (1955) used the transformation in his study and found the solution in closed analytical form, except for an inverse transformation back to physical space. For our two-layer model, the following transformation is introduced

$$\mathrm{d}\psi_1 = h_1 v_1 \,\mathrm{d}x. \tag{2.16}$$

In the new streamfunction coordinate ψ_1, (2.7) and (2.11) become

$$\frac{\mathrm{d}v_1^2}{\mathrm{d}\psi_1} = 2\left[F_1(\psi_1) - \frac{f}{h_1}\right], \tag{2.17}$$

$$\frac{\mathrm{d}\psi_2}{\mathrm{d}\psi_1} = \frac{h_2 v_2}{h_1 v_1}. \tag{2.18}$$

Eqs. (2.17, 2.18) and (2.13, 2.9, 2.10) can be thought of as a numerical coordinate transformation, including variables h_1, v_1, h_2, v_2, and ψ_2. It is remarkably simpler than the original system. In fact, instead of six first-order differential equations, there are only two in the new system. Most importantly, the new equations are non-stiff and the boundary conditions are posed over a finite domain $[0, \psi_{1\infty}]$.

At each latitude the system can be non-dimensionalized using the interior solution at this latitude

$$x = \frac{\sqrt{g' h_{1\infty}^*}}{f^*} x', \quad y = \frac{f_0}{\beta} y',$$

$$\begin{aligned}
& f = f^* f', \quad f' = \frac{1 + y'}{1 + y'^*}, \\
& h_1 = h_{1\infty}^* h_1', \quad h_2 = k h_{1\infty}^* h_2', \\
& \psi_1 = \frac{g' h_{1\infty}^{*2}}{f^*} \psi_1', \quad \psi_2 = \frac{g' h_{1\infty}^{*2}}{f^*} \psi_2', \\
& v_1 = \sqrt{g' h_{1\infty}^*}\, v_1', \quad v_2 = \sqrt{g' h_{1\infty}^*}\, v_2', \\
& F_1 = \frac{f^*}{h_{1\infty}^*} F_1', \quad F_2 = \frac{f^*}{h_{1\infty}^*} F_2', \\
& G_1 = h_{1\infty}^* G_1', \quad G_2 = h_{1\infty}^* G_2',
\end{aligned} \tag{2.19}$$

where $h_{1\infty}$ and $h_{2\infty}$ are the layer thicknesses of the mid-ocean thermocline, f^* is the Coriolis parameter at latitude y^* and $k = h_{2\infty}^*/h_{1\infty}^*$. Finally, after dropping the primes over the new non-dimensional variables, we have the set of working equations corresponding to (2.17, 2.18, 2.13, 2.9, 2.10)

$$\frac{\mathrm{d}v_1^2}{\mathrm{d}\psi_1} = 2\left[F_1(\psi_1) - \frac{1}{h_1}\right], \tag{2.20}$$

$$\frac{\mathrm{d}\psi_2}{\mathrm{d}\psi_1} = k\frac{h_2 v_2}{h_1 v_1}, \tag{2.21}$$

$$\frac{\gamma}{2} h_1^2 + k h_1 h_2 + \frac{k^2}{2} h_2^2 = \frac{\gamma}{2} + k + \frac{k^2}{2} - (\psi_{1\infty} + \psi_{2\infty} - \psi_1 - \psi_2), \tag{2.22}$$

$$\frac{1}{2} v_1^2 + \gamma h_1 + k h_2 = G_1(\psi_1), \tag{2.23}$$

$$\frac{1}{2} v_2^2 + h_1 + k h_2 = G_2(\psi_2), \tag{2.24}$$

with boundary conditions

$$\begin{aligned}
& h_1(\psi_{1\infty}) = h_2(\psi_{1\infty}) = 1, \\
& v_1(\psi_{1\infty}) = v_2(\psi_{1\infty}) = 0, \\
& \psi_2(0) = 0, \quad \psi_2(\psi_{1\infty}) = \psi_{2\infty}.
\end{aligned} \tag{2.25}$$

These equations can be solved by a shooting method. If $h_{1\mathrm{w}}$ (the upper layer thickness at the western wall) is guessed, $h_{2\mathrm{w}}$ can be calculated by (2.22) and $v_{1\mathrm{w}}$, $v_{2\mathrm{w}}$ by (2.23, 2.24), thus (2.20) and (2.21) can be integrated (using a fourth-order Runge-Kutta method) from $\psi_1 = 0$ towards $\psi_1 = \psi_{1\infty}$. Generally, this integration process will be interrupted at $\psi_1^{\mathrm{inp}} < \psi_{1\infty}$ where v_1^2 or v_2^2 first becomes non-positive. $h_{1\mathrm{w}}$ can be repeatedly adjusted until ψ_1^{inp} converges to $\psi_{1\infty}$ and ψ_2, h_1, h_2, v_1, and v_2 converge to their corresponding values at infinity ($\psi_{1\infty}$).

For some parameters the numerical coordinate transformation may fail to converge, in such cases a similar coordinate transformation based on ψ_2 or $\psi = \psi_1 + \psi_2$ can be used instead of ψ_1. For the cases studied here these coordinate transformations have been very successful.

3. Searching for continuous solutions

As a confirmation of the numerical scheme and the computer program, the classical case of constant potential vorticity with $\gamma = 2$ and equal layer thickness in the interior discussed by Blandford (1965) is recalculated and shown in Fig. 1. The solution appears as two branches. The southern branch starts from $y = 0$ and extends to $y = 0.4635$. The northern branch starts from $y = 0.45$ and extends to $y = 0.875$, and at both ends the lower layer thickness vanishes. As noted by Blandford, within region $y \in [0.45, 0.463]$ there are three solutions. Our numerical results are exactly the same as Blandford's analytical solution.

In fact, the southern branch of the solution breaks down at $y = 0.463$, where the upper layer thickness at the western wall $h_{1\text{w}}$ is non-zero, but its meridional gradient $\mathrm{d}h_{1\text{w}}/\mathrm{d}y$ becomes unbounded. This branch is non-physical because the latitude variation of layer thickness is discontinuous. Although there is another solution belonging to the northern branch, indicated by the long-dashed line in Fig. 1, this branch is non-physical because it is unconnected to the southern part of the western boundary where the inertial boundary current first formed. For this parameter set no smooth physical solution over the domain $y \in [0, 1]$ exists.

In the following experiments, the potential vorticity of the incoming interior flow is changed by varying the slope of the interfaces at infinity. First, we will keep the layer thickness at $y = 1$ ($h_{1\infty n}$ and $h_{2\infty n}$) and the lower interface unchanged. Thus, in dimensional form

$$h_{1\infty} = h_{1\infty n}[1 + \alpha_1(y - 1)],$$

$$h_{2\infty} = h_{2\infty n}[1 + \alpha_2(y - 1)].$$

As the lower interface is fixed, $\alpha_1 + \alpha_2 = 1$ is maintained. From physical intuition, the early "separation" of the solution discussed above implies that the inertial boundary current is unable to carry the large volume flux. If the upper interface slope is reduced, the total mass flux in the upper layer declines, thus the separation of

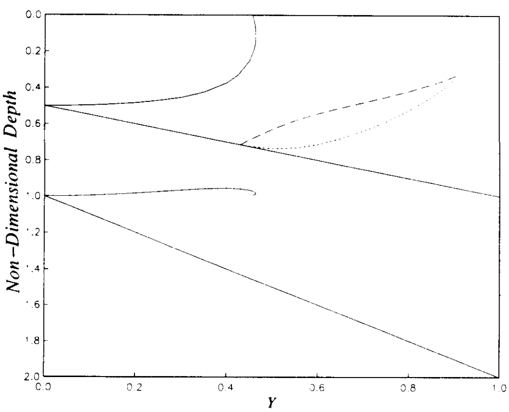

Fig. 1. Meridional views of a model of constant potential vorticity. Two solid straight lines indicate the upper and lower interfaces in the interior, two solid curves show the corresponding interfaces on the western wall (the southern branch), the long-dashed line indicates the upper interface and the short-dashed line depicts the lower interface belonging to the northern branch.

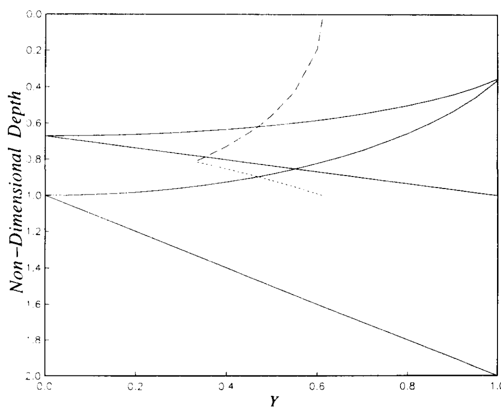

Fig. 2. Meridional views of a model of non-constant potential vorticity. Two solid straight lines indicate the upper and lower interfaces in the interior, two solid curves show the corresponding interfaces on the western wall. Note that the southern branch joins with the northern branch smoothly, while the long-dashed and the short-dashed lines indicate the upper and lower interfaces of the spurious solution.

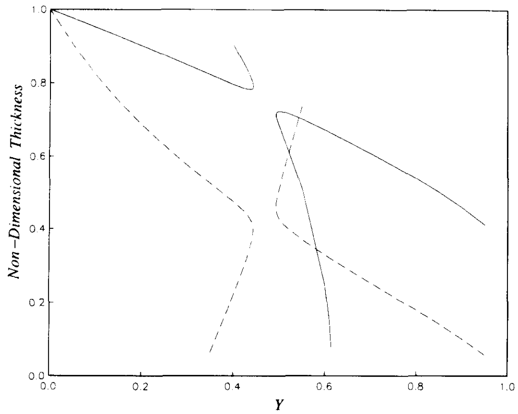

Fig. 3. The solution separates into upper and lower branches for supercritical parameters. Solid (dashed) lines indicate the upper (lower) interface at the western wall. Note that layer thicknesses are non-dimensionalized using the interior layer thicknesses at each latitude.

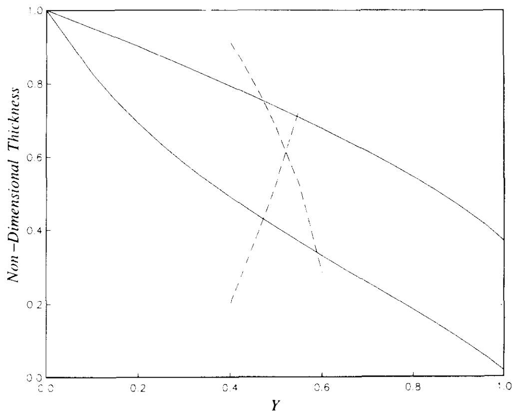

Fig. 4. Two branches join smoothly again as the lower interface slope is reduced. Solid lines indicate the upper and lower interface at the western wall, and dashed lines indicate the spurious branches.

the upper layer may be postponed. In fact, as α_1 (the upper layer slope) decreases, the "separation" latitude of the solution's southern branch moves northward and the gap between the two branches diminishes. At critical values ($\alpha_1 = 0.3287375$, $\alpha_2 = 0.6712625$) the southern and northern branches join smoothly at a critical point $y = 0.4700$ and form a physical solution continuously extending over $y \in [0, 1]$, as indicated by two solid curves in Fig. 2. Note that the solution is very smooth near $y = 1$, thus a smooth solution with the lower layer separated seems to exist beyond $y = 1$, although details of the solution involving a separated lower layer require closer examination in a further study. There is also a spurious solution which is disconnected from the southern boundary, as indicated by dashed lines in Fig. 2.

As the upper interface slope is further reduced, the solution separates into an upper and a lower branch, as shown in Fig. 3 for $\alpha_1 = 0.325$ and $\alpha_2 = 0.675$. The upper branch extends from $y = 0$ to $y = 0.4430$. Within a small distance south of $y = 0.4430$, the upper branch has two solutions at each latitude. Moreover, $\mathrm{d}h_{1w}/\mathrm{d}y$ is unbounded at $y = 0.4430$. There is no solution within a narrow latitude band $y \in [0.4430, 0.4925]$. Both the two branches are non-physical and there is no physical solution extending over $y \in [0, 1]$ for this parameter set.

In the discussion above, only the upper interface slope has been changed. Varying the lower interface slope has a similar effect. In fact, the two separated branches shown in Fig. 3 can be brought together again by changing the lower interface slope but fixing the upper interface. This time we will keep the layer thickness at $y = 0$ ($h_{1\infty s}$ and $h_{2\infty s}$) unchanged, thus the (dimensional) layer thicknesses of the mid-ocean thermocline are

$$h_{1\infty} = h_{1\infty s}(1 + a_1 y), \quad h_{2\infty} = h_{2\infty s}(1 + a_2 y).$$

For the case shown in Fig. 3,

$$\frac{h_{1\infty s}}{h_{2\infty s}} = \frac{27}{13} \approx 2.07692, \quad a_1 = \frac{0.65}{1.325},$$

$$a_2 = \frac{27}{13} \approx 2.07692.$$

If a_1 remains unchanged but a_2 is gradually reduced, the upper branch approaches the lower branch. At a critical value $a_2 = 2.0239478$, the two branches join smoothly at a critical point $y = 0.4715$ and form a continuous solution, as shown by two solid curves in Fig. 4.

For a_2 smaller than this critical value, the two branches separate again and appear in the form of a southern and a northern branch. Fig. 5 shows enlarged maps of this separation phenomenon for the case of $a_2 = 2.021$. The small crosses in Fig. 5b are calculated points of the solution with separated branches, indicating the branching-off of the lower layer. As a_2 is decreased further, the separation between the two branches becomes even larger.

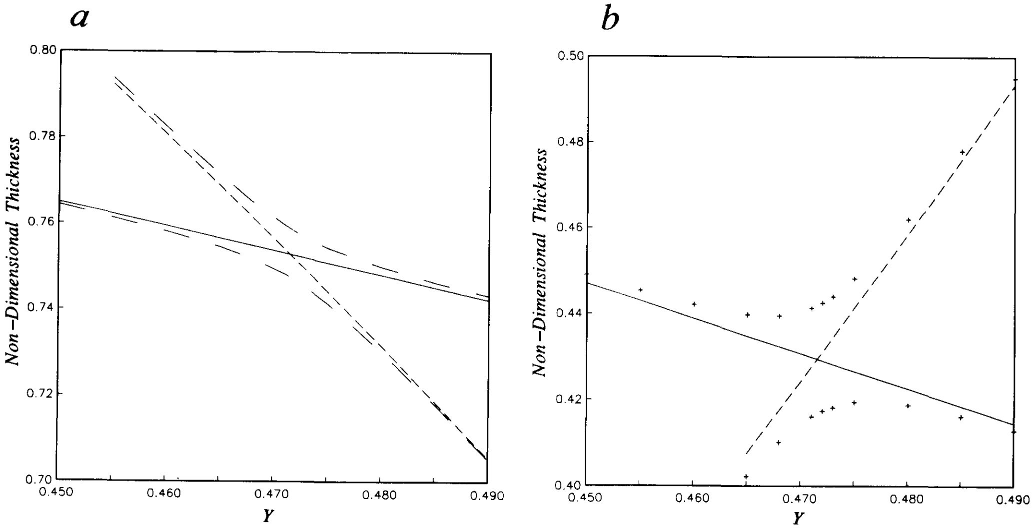

Fig. 5. Departure of the solution as the parameters deviate from the critical values, solid lines and short-dashed lines indicate the physical and spurious solutions shown in Fig. 4. (a) The upper interface at the western wall, long-dashed lines depict two branches of the solution for a case with non-critical parameters. (b) The lower interface at the western wall, crosses represent lower interface at the western wall for a case of non-critical parameters.

The structure of the inertial western boundary current structure at different sections for the case of Fig. 4 is shown in Figs. 6 and 7. Most importantly, these figures demonstrate the usefulness of the streamfunction coordinate transformation introduced in this study. The structure of the inertial boundary current is clearly shown for the entire width of the boundary current, up to $\psi_1 = \psi_{1\infty}$, which corresponds to $x = \infty$ in physical space. Given the stiffness of the original equations in physical coordinates, numerical solutions calculated using these equations would have diverged very quickly a short distance from the coast, due to small truncation errors in calculations. The numerical calculations have been carried out on a Sun Workstation 3/50. Using double precision and $\Delta\psi_1 = 0.002\psi_{1\infty}$ in the Runge-Kutta integration, ψ_1, ψ_2, h_1, and h_2 all converge to their corresponding values at $\psi_1 = \psi_{1\infty}$ with relative errors less than 0.004. These errors can be further reduced by using a smaller step for $\Delta\psi_1$. Fig. 6 shows a smooth structure developing within the western boundary current from $y = 0.25$ to $y = 0.85$. As the current moves northward, layer thickness at the coast decrease, while the velocity along the coast increases due to decrease of the Bernoulli head. In comparison, a section of the spurious branch taken at $y = 0.55$ is also included, Fig. 6d. This should be compared with the physical branch at the same latitude, Fig. 6b.

Figs. 6a and 6c show the structure of an inertial western boundary current at different sections along the western coast. For comparison, we define the outer edge of the boundary current as the streamline $\psi_1 = 0.95\psi_{1\infty}$. At section $y = 0.25$, the boundary edge is at $x = 3.366$, where $h_1 = 0.993$, $h_2 = 0.985$, $\psi_2 = 0.947$, $v_1 = 0.016$, $v_2 = 0.012$. At $y = 0.85$, the boundary edge is at $x = 1.342$, where $h_1 = 0.981$, $h_2 = 0.971$, $\psi_2 = 0.940$, $v_1 = 0.044$, $v_2 = 0.031$. Note that x is in non-dimensionalized coordinates using the local Rossby deformation radius $r_1(y) = \sqrt{g' h_{1\infty}}/f$. Taking into account the difference in r_1, we have an estimation that the width of the inertial western boundary current decreases to 1/3.31 from section $y = 0.25$ to section $y = 0.85$. Accordingly, all other dynamical fields of the boundary current are intensified.

The streamline patterns of the inertial western boundary current are presented in Fig. 7. This figure is based on calculations at 20 longitudinal sections, the streamline interval is 1/20 of the total volume flux from the interior at the northern section $y = 1$. The right hand end of each streamline should have been extended to infinity; however, due to the finite resolution used in the calculation, most lines stop shortly beyond $x = 1$.

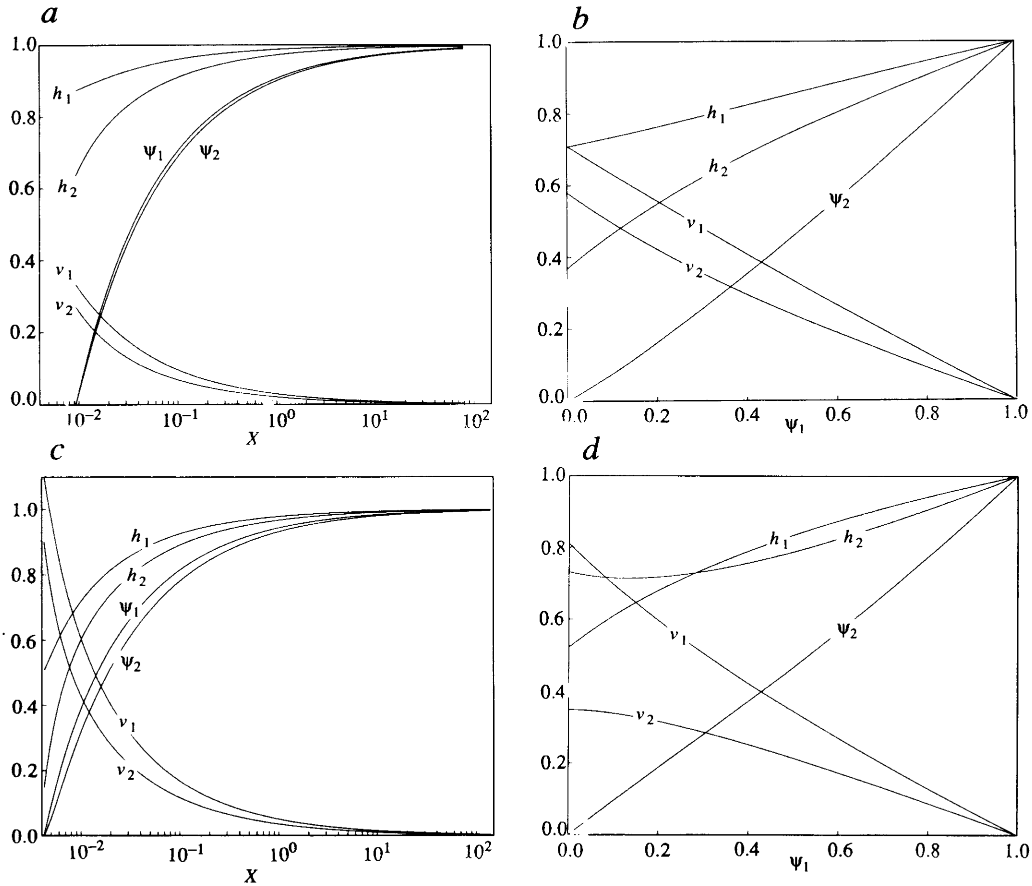

Fig. 6. Boundary layer structure at different sections in non-dimensional units, (a) $y = 0.25$; (b) $y = 0.55$; (c) $y = 0.85$; (d) $y = 0.55$ (for the spurious solution). Ordinate in (a) and (c) is in physical space, non-dimensionalized by the Rossby deformation radius at each section; ordinate in (b) and (d) is in the non-dimensional streamfunction of the upper layer.

To show the boundary structure clearly, this figure is drawn in logarithmic scale based on the Rossby deformation radius of the first layer r_1, calculated at the northern boundary of the model. There is slight crossover of the streamlines in the two layers, especially near the northern boundary where the lower layer will soon be separated from the coast.

4. Classifying the solutions on a phase plane

In this section we will search through parameter space for continuous solutions. For simplicity, we will assume that $\gamma = 2$ and layer thicknesses remain of one unit at the southern boundary. Thus, the (dimensional) layer thicknesses are:

$$h_{1\infty} = 1 + a_1 y, \quad h_{2\infty} = 1 + a_2 y,$$

where a_1 and a_2 are the only parameters of the model. The structure of the incoming flow is schematically depicted in an inset figure in the right side of Fig. 8. Note that layer thicknesses of the interior flow can be non-dimensionalized by the upper layer thickness at the latitude of concern y^*, thus in the final non-dimensional notation the layer thicknesses are

$$h_{1\infty} = \frac{(1 + a_1 y)}{(1 + a_1 y^*)}, \quad h_{2\infty} = \frac{(1 + a_2 y)}{(1 + a_2 y^*)},$$

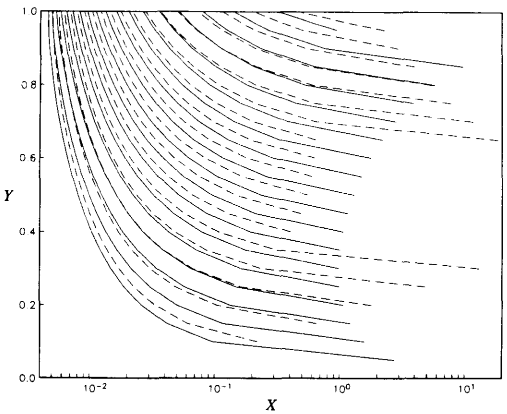

Fig. 7. Streamline patterns in the upper layer (solid lines) and lower layer (dashed lines), the ordinate is in units of the Rossby deformation radius at the northern boundary of the model ($y = 1$).

and F_1, F_2, G_1, G_2 can be written in parametric forms

$$F_1 = \frac{(1 + a_1 y^*)(1 + y)}{(1 + a_1 y)(1 + y^*)},$$

$$F_2 = \frac{(1 + a_1 y^*)(1 + y)}{(1 + a_2 y)(1 + y^*)},$$

$$G_1 = \frac{\gamma + 1 + (\gamma a_1 + a_2) y}{1 + a_1 y^*}, \quad G_2 = \frac{2 + (a_1 + a_2) y}{1 + a_1 y^*},$$

$$\psi_1 = \frac{(\gamma a_1 + a_2)(1 + y^*)}{(1 + a_1 y^*)^2} [a_1 y + (1 - a_1) \ln(1 + y)],$$

$$\psi_2 = \frac{(a_1 + a_2)(1 + y^*)}{(1 + a_1 y^*)^2} [a_2 y + (1 - a_2) \ln(1 + y)].$$

The global structure of the system is best represented by the non-dimensional upper layer thickness at the western wall. The abscissa in Fig. 8 is the non-dimensional slope of the upper layer and the ordinate is that of the lower layer. The origin of the coordinates for each small embedded figure indicates the interface slopes of the interior solution, a_1 and a_2. In each small figure, the abscissa is the non-dimensional northward distance y, and the ordinate is the non-dimensional upper layer thickness at the western

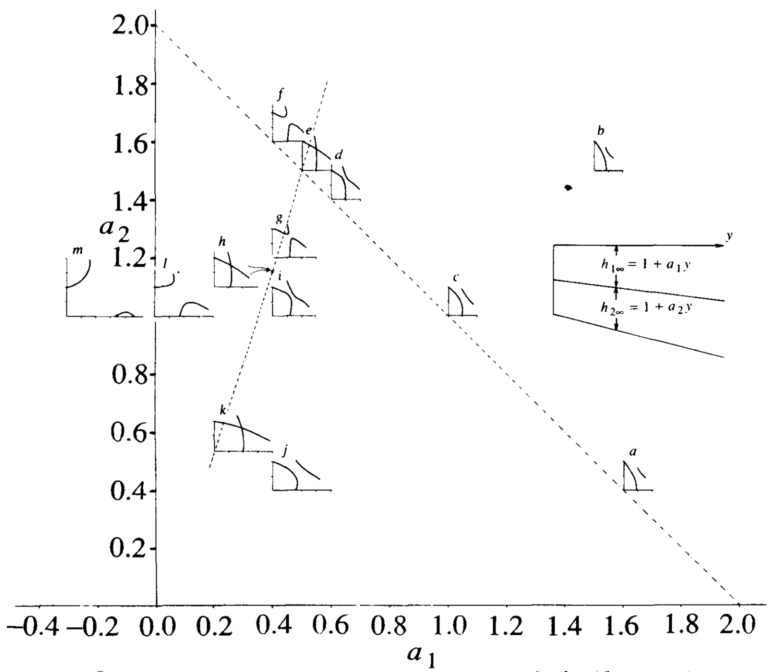

Fig. 8. Solution classification of a two-moving layer model on a phase plane. Small figures depict the non-dimensionalized upper layer thickness at the western wall for different parameters (interfacial slopes). A dashed line indicates the critical line which separates the phase plane into two regions. Solutions within each region have similar structure.

wall. One grid represents 0.5 non-dimensional unit, respectively. The dot–dashed line indicates the choice of fixing the lower interface the same as the case of constant potential vorticity and equal thickness in both layers.

The first three cases, (a), (b), and (c), represent cases of large upper interfacial slope. Case (c) of $a_1 = a_2 = 1$ is the well-known case of constant potential vorticity in both layers discussed by Blandford (1965). Potential vorticity in the upper layer decreases northward in both cases (a) and (b). However, potential vorticity in the lower layer increases northward in case (a). In all three cases the solution appears in the form of two separate branches. The southern branch starts from the southern boundary, $y = 0$, and extends northward. This branch of solution breaks down before it reaches $y = 0.5$. At latitude y_m, the meridional gradient of the upper layer thickness at the western wall becomes unbounded, $dh_{1w}/dy = -\infty$. In fact, south of y_m there may be two or even three possible solutions at each latitude, two of them belong to the southern branch, and the third one belongs to the northern branch. The northern branch extends towards $y = 1.0$, but for these three cases it vanishes before reaching $y = 1.0$ at a point where the second layer separates from the western wall. These solutions are non-physical, since the latitudinal variation of layer depth is not continuous.

We have included several cases in which the lower interface remains fixed at infinity, but the upper interfacial slope is reduced gradually from cases (a) to (c), (d), (e), and (f). It is readily seen that as the upper interfacial slope is reduced, the two branches of the solution move towards each other. Finally, at critical parameters ($a_1 = 0.50608$, $a_2 = 1.49392$) the two branches join at a critical point, $y_c = 0.511$, and form a continuous solution extending from $y = 0$ to $y = 0.98$, as shown in case (e). It is important to note that as the model approaches a critical state, an angular point develops along each branch of the solution, and at the critical parameters the two branches actually join at the critical point where both branches have discontinuity in their first derivative. Beyond the critical parameters solutions of the model emerge in the form of an upper and lower branch, see case (f).

Another series of cases also show how the solutions evolve as the lower interfacial slope changes. From case (f) to (g), (h), (i), and (j), the slope of the upper interface is fixed at $a_1 = 0.4$, while the lower interfacial slope is reduced from $a_2 = 1.6$ to 0.4. It is readily seen that as a_2 is reduced, the upper and lower branches approach each other. At a critical parameter $a_2 = 1.15144$ the two branches join at a critical point $y_c = 0.598$ and form a smooth solution extending from $y = 0$ to 1.2, see case (h). Beyond this critical value, the solution separates into two branches again, see cases (i) and (j). The southern branch has the same structure as cases (a), (b), (c), and (d) discussed above.

For cases of small or negative upper interfacial slope, it is more convenient to use a coordinate transformation based on the streamfunction of the lower layer as discussed in Section 2. Generally, as the upper interfacial slope becomes zero or negative, the separation of the two branches of the solution increases. Case (l) shows the solution of zero upper interfacial slope. This case represents the situation when zonal velocity of the interior flow is the same in both layers. The non-dimensional upper layer thickness at the western wall of the southern branches increases northward.

As the upper interface slope becomes negative, the two branches of the solution move farther away from each other, see case (m). Blandford (1965) speculated that a solution with a countercurrent in the upper layer might exist for such situations. We have been, however, unable to find any countercurrent in the solution.

From Fig. 8, it is clear that the phase plane can be divided into two regions by a critical line. On the left part of the phase plane, solutions of the model appear as upper and lower branches separated by a band. The degree of separation of the two branches can be roughly described in terms of the "distance" between the two branches, i.e., the minimum distance between points belonging to different branches. As the model parameters approach those along the critical line, the distance between two branches decreases. Along (and only along) the critical line the distance vanishes and two branches join smoothly at a critical point. The location of the critical point depends no parameter values. As the interfacial slopes decrease, mass fluxes contained in the boundary layers also decrease and boundary layers should stick to the wall longer before separation or interruption occurs. This can be seen clearly from Fig. 8, where the critical point gradually moves from $y_c = 0.511$ for case (e) to $y = 0.598$ for case (h). Finally, as a_1 and a_2 decrease to 0.2 and 0.5 respectively, y_c becomes 0.951 in case (k).

To the right of the critical line the solutions of the model appear in the form of southern and northern branches as described above. As parameters of the model deviate from those on the critical line, the distance between two branches of the solution increases too.

Note that the northward potential vorticity gradient is positive in both layers for cases (k) and (j), but it is negative in the lower layer for cases (d), (e), (f), (g), and (h). Therefore, the continuity through the critical point of the solutions does not seem to have a simple direct connection with the stability of the incoming flow, although the physical cause of this phenomenon is not yet clear.

We have run other experiments in which the density jumps across interfaces, layer thickness ratio at the southern boundary are different from the cases discussed above, including several cases of non-constant interfacial slopes. Our preliminary results indicate that the structure of the model's solutions remains basically the same, although the position of the critical line can change with the alteration of the parameters.

5. Conclusion

Since Blandford's (1965) study, a major concern has been whether a two-moving-layer inertial boundary current fed from the subtropical gyre interior possesses solutions extending to reasonably high latitude without interruption or separation. Using a streamfunction coordinate transformation, we have found continuous solutions for special sets of parameters. In fact, in the phase plane of a simple model exists a critical line separating the phase plane into two regions. Within each region, solutions of the model have similar structure, i.e., they appear in the form of two unjoined south/north (upper/lower) branches. The south (upper) branch breaks down much farther south than expected from physical intuition. Thus, within these two regions the system has no physical solution which can extend continuously to high latitude. However, if the parameters are gradually modified towards those along the critical line, these two branches can be brought towards each other. In fact, for parameters along the critical line, these two branches join smoothly and form a physical solution which extends to high latitude without interruption.

This system shares some similarity with the virtual control phenomenon in the one-dimensional hydraulic problem as discussed by Wood (1968) and the zero potential vorticity model by Luyten and Stommel (1985). Our preliminary numerical study also indicates that the global structure of the model's solution remains basically the same for general cases of different density jumps at the interfaces, different layer thickness ratios at the southern boundary and even non-constant interfacial slopes. So far, we have been unable to unravel the physical nature of this critical condition nor state the constraint over the mid-ocean thermocline in a concise way. Nevertheless, the physical meaning of our study is very clear that the continuity of a multi-layer inertial western boundary current affects the structure of the mid-ocean thermocline. If a two-moving-layer inertial western boundary current is to be continuous through a critical point, the thermocline structure in the mid-ocean must satisfy some consistency constraints. Since the inertial boundary current plays an important role in setting up the circulation in a closed basin, it seems obvious that it should affect the structure of the mid-ocean thermocline. On the other hand, frictional western boundary currents do not seem to play a similar role, apparently due to a loss of information in diffusive processes.

This study is a step towards closing an ideal-fluid thermocline model with an inertial western boundary current at the western wall. Our study of the present model raises hope that it is possible to find continuous solutions of multi-layered inertial western boundary currents which can match the interior wind-driven circulation calculated by the Luyten et al. model. Matching an interior flow driven by specified wind stress with an inertial western boundary current in a multi-layer model is currently underway and will be published in a separate paper.

Our success in tracking down the exact solutions also shows the power of the integral coordinate transformation introduced in this study. Stiff equations over an infinite domain have been a real challenge for numerical study. However, in the present case, we are able to reduce this difficult problem to solving stable equations over a finite domain. Although the coordinate transformation needs some elaboration for cases involving countercurrents, its usefulness for general stiff equations in other branches of science and engineering should be explored in further studies.

6. Acknowledgements

I have greatly benefited by discussion with many of my colleagues at Woods Hole. My interest in this problem was stimulated by the work of J. Luyten and H. Stommel, and this study would have never been completed without the encouragement of H. Stommel and N. Hogg. R. Samelson and two reviewers' comments were very helpful in clarifying the presentation. My research work has been supported by the National Science Foundation through grant OCE88-08076.

REFERENCES

Blandford, R. R. 1964. *Inertial flow in the Gulf Stream*. California Institute of Technology Doctoral Thesis, 152 pp.

Blandford, R. R. 1965. Inertial flow in the Gulf Stream. *Tellus 17*, 69–76.

Charney, J. G. 1955. The Gulf Stream as an inertial boundary layer. *Proceedings of the National Academy of Science, USA 41*, 731–740.

Gear, C. W. 1971. *Numerical initial value problems in ordinary differential equations*. Prentice-Hall, Englewood Cliffs, New Jersey, 253 pp.

Huang, R. X. 1988. On boundary value problems of the ideal-fluid thermocline. *J. Phys. Oceanogr. 18*, 619–641.

Luyten, J. R., Pedlosky, J. and Stommel, H. 1983. The ventilated thermocline. *J. Phys. Oceanogr. 13*, 292–309.

Luyten, J. and Stommel, H. 1985. Upstream effects of the Gulf Stream. *Prog. Oceanogr. 14*, 387–399.

Mises, R. Von. 1927. Bemerkungen zur Hydrodynamik. *Z. Angew. Math. Mech. 7*, 425–431.

Stommel, H. 1954. Discussion at the Woods Hole Convocation, June, 1954. *J. Mar. Res. 14*, 504–510.

Wood, I. R. 1968. Selective withdrawal from a stably stratified fluid. *J. Fluid Mech. 32*, 209–223.